Journal of Magnetism and Magnetic Materials 473 (2019) 403–409

Contents lists available at ScienceDirect

Journal of Magnetism and Magnetic Materials

journal homepage: www.elsevier.com/locate/jmmm

Research articles

Specific loss power measurements by calorimetric and thermal methods on γ-Fe_2O_3 nanoparticles for magnetic hyperthermia

Marco Coïsson[a,*], Gabriele Barrera[a], Carlo Appino[a], Federica Celegato[a], Luca Martino[a], Alexander P. Safronov[b,c], Galina V. Kurlyandskaya[b,d], Paola Tiberto[a]

[a] INRIM, Nanoscience and Materials Division, Torino, Italy
[b] Ural Federal University, Ekaterinburg, Russia
[c] Institute of Electrophysics UD RAS, Ekaterinburg, Russia
[d] University of Basque Country, Leioa, Spain

ARTICLE INFO

Keywords:
Magnetic hyperthermia
Fe-oxide
Magnetic nanoparticles

ABSTRACT

Specific loss power has been measured on γ-Fe_2O_3 nanoparticles dispersed in water by means of several techniques, i.e. heat flow in a calorimeter, hyperthermia, and static and dynamic hysteresis loops. Static hysteresis loops as a function of the maximum applied field underestimate the power losses as dynamic effects are not exploited, but turned out to be a valuable tool to prove the consistency of specific loss power measurements obtained by the other techniques over a wide range of applied magnetic field intensities. A temperature-dependence of the specific loss power has been taken into account in hyperthermia measurements performed with a fully modelled non adiabatic experimental setup. Simple mean-field theoretical models (interacting superparamagnetic, modified Stoner-Wohlfarth) have been exploited to reproduce the static energy losses of the particles.

1. Introduction

Magnetic nanoparticles (MNPs) are attractive materials for numerous biomedical applications, from magnetic imaging and hyperthermia to biosensing and regenerative medicine [1–5]. They attracted special interest as their movements can be controlled by external magnetic field gradients, and can be exploited as carriers of drugs toward a targeted region [6]. MNPs may also transfer the energy of time varying magnetic fields, therefore heating up their local environment and consequently serving as hyperthermia agents: they are therefore potentially exploitable for contributing to the cancer treatment [7].

Biomedical applications of nanomaterials, including nanoparticles, require their thorough characterisation by different techniques because all properties at nanoscale can vary from batch to batch. Special strict rules are applied to preclinical physicochemical characterisation of MNPs which includes size, shape, aggregation and/or agglomeration grade definition not only for each batch but also for certain time period [7–9]. Even though iron oxide MNPs can be produced by different techniques with well controllable sizes from a few nanometers to a few tens of nanometers, comparable with or smaller than biological units such as cells, viruses or proteins, manufacturing techniques providing enhanced batch sizes attract special attention [7]. Among others, one can mention electrophysical techniques such as electric explosion of wires which has production rates up to 200 g/h, and laser target evaporation method (LTE) [10] which provides production rates up to 50 g/h [11,12]. Both above mentioned techniques ensure fabrication of spherical MNPs.

Ferrofluids [13–15] or stable colloidal dispersions of de-aggregated MNPs in water are a most compatible way to provide MNPs for living systems [6,16–18]. However, their characterisation by means of standardised techniques is still a challenge [19]; the tasks required to reliably characterise magnetic hyperthermia materials are discussed in depth in [20]. For example, even though several techniques are available for the measurement of the specific loss power of Fe-oxide MNPs based suspensions, their thorough comparison and analysis of advantages and disadvantages is still rare in the research literature.

Therefore, in this paper we have addressed the subject of Fe-oxide MNPs for biomedical applications, specifically for magnetic hyperthermia [21–26], through a multi-faceted approach. The magnetic nanoparticles have been prepared with the promising technique of laser target evaporation, which allows the production of large, uniform batches, whereas their specific loss power has been measured with three different techniques: thermal measurements in a custom-built

* Corresponding author.
E-mail address: m.coisson@inrim.it (M. Coïsson).

https://doi.org/10.1016/j.jmmm.2018.10.107
Received 21 June 2018; Received in revised form 17 October 2018; Accepted 22 October 2018
Available online 23 October 2018
0304-8853/ © 2018 The Authors. Published by Elsevier B.V. This is an open access article under the CC BY-NC-ND license (http://creativecommons.org/licenses/BY-NC-ND/4.0/).

hyperthermia setup, calorimeter measurements, and dynamic hysteresis loops. In order to compare the results obtained by thermal and calorimetric setups, spanning applied magnetic fields of very different intensities, static hysteresis loops have been exploited; they easily cover very large field intensity intervals, and proved to offer a good way to link specific loss power measurements, even though they lack any contribution due to dynamic effects. Simple mean-field models have also been exploited to describe the energy losses of the ensemble of MNPs. The selected fabrication technique is crucially important for the achievement of the desired results of comparative analysis, as a relatively large amount of material is necessary for such comparison. The available data on the LTE MNPs, acquired with several different techniques, allow us to gather a deep and comprehensive understanding of their functional properties for hyperthermia applications.

2. Experimental

The studied sample is composed of γ-Fe_2O_3 particles obtained by laser target evaporation [12]. The exact chemical composition of the particles was determined by the combination of the analysis of the spinel lattice period provided by X-ray diffraction and Red-Ox titration [9,27]. The crystalline structure of fabricated nanoparticles was identified as the inverse spinel l with a space group Fd3m. The lattice period a was found to be about 0.8358 nm, which was larger than that for maghemite (γ-Fe_2O_3, $a = 0.8346$ nm) but lower than that for magnetite (Fe_3O_4, $a = 0.8396$ nm). Based on the dependence between the lattice period of the spinel unit cell and the effective state of oxidation of Fe, the composition of the nanoparticles was defined as 76% of γ-Fe_2O_3 and 24% of Fe_3O_4 and will be referred in the following as γ-Fe_2O_3 or maghemite for simplicity.

The weighted d_w and number d_n average diameters, respectively equal to 18.5 nm 11.0 nm, were calculated as follows:

$$d_w = \frac{\Sigma d_i^4 N_i}{\Sigma d_i^3 N_i}$$
$$d_n = \frac{\Sigma d_i N_i}{\Sigma N_i} \quad (1)$$

where N_i is the number of particles in the i-th fraction and d_i is the particle diameter in the i-th fraction. The obtained values of d_n and d_w differ from each other as it usually happens for polydisperse particle size distributions [9,27]. 2164 particles were counted for the evaluation of size distribution function. The histogram was fitted by a lognormal distribution function [28] with the median value 11.7 nm and a standard deviation for the natural logarithm of the diameter $\sigma = 0.423$ (unitless). The geometric standard deviation [29], which is the exponential function of σ, has a value of 1.527, which means that the diameters in the set deviate in average by 52.7% from the median. The correlation coefficient for the fitting was $R^2 = 0.989$.

In order to reach colloidal stability, electrostatic stabilization of the suspension was ensured with the following procedure. The particles were then dispersed in 5 mM water solution of Na citrate. Stock dispersion was 6% (percentages are in weight) considering magnetic nanoparticles and 0.2% considering citrate. Dispersion was exhaustively treated by ultrasound: 250 min in a laboratory ultrasound bath and then 30 min in Cole-Parmer ultrasound processor CPX-750 operated at 250 W output. Then the dispersion was centrifuged at 8000 rpm for 5 min. The supernatant was taken out and used further. The concentration of magnetic Fe-oxide particles in the supernatant ferrofluid was evaluated based on the dry residue after evaporation of water to constant weight. The dry residue was 5.2% including magnetic nanoparticles and citrate. Presuming that the concentration of citrate (0.2%) does not change in the treatment, the final concentration of magnetic nanoparticles in ferrofluid was 5.0%. Fig. 1 shows a TEM image (JEOL JEM2100 microscope operated at 200 kV) of the particles, together with their size distribution. Additionally, hysteresis loops measured with a vibrating sample magnetometer are reported both on a dry particles sample and on one where particles are dispersed in water. Coercive fields, not visible in the figure because of the chosen horizontal scale, are of $\approx$ 800 A/m for the dried sample, and $\approx$ 200 A/m for the water dispersed particles. These coercive field values, obtained in static conditions, although not large, demonstrate that the nanoparticles are not in a superparamagnetic state at room temperature, therefore leading to mechanisms of power losses mainly related to their hysteresis properties. They can be either in an interacting superparamagnetic regime, or in a blocked (Stoner-Wohlfarth) regime, as it will be discussed later. It is interesting to note that the magnetic susceptibility of the water-dispersed particles is larger and the coercivity smaller than those of the dry particles, because the particles are free to move and rotate in the fluid, therefore responding more easily to the applied static magnetic field.

Hyperthermia measurements have been conducted using a custom-built setup [30] consisting in an rf coil operating at 100 kHz capable of generating an electromagnetic field with magnetic field intensity in the range 24 − 80 kA/m (see Fig. 2). The actual applied field values have been 24, 32, 40 and 48 kA/m. The coil is water cooled at a temperature that is kept constant at $\approx$ 22 °C. The temperature T_w of the water suspension containing the nanoparticles (having a volume of 1 mL) is measured by means of a fibre optic thermometer. T_w *vs.* time curves are recorded for the whole duration of the experiment, which consists in switching on the electromagnetic field when the temperature of the water suspension is stable at room temperature, and switching it off after 3600 s. The temperature of the water suspension is measured both during the heating process (when the field is on) and the subsequent cooling (when the field is off).

The $T_w(t)$ experimental curve is then reproduced by numerically solving a set of coupled differential equations reported in [31]. The equations are derived from a simple thermodynamical model taking into account the heat flow from the suspension to the sample holder, and from the sample holder to the outside environment. The sample holder is meant to act as a thermostat against temperature fluctuations. The set of coupled differential equations have the temperatures $T_s(t)$, $T_w(t)$ and $T_h(t)$ as unknowns, of which $T_w(t)$ is of interest as it is the quantity that is directly measured in hyperthermia experiments. The heat flow mechanisms among the different components of the system are taken into account through a set of parameters appearing in the differential equations that are determined by appropriate calibration [31]. Upon solving the equations, the only free parameter that is adjusted to reproduce the experimental data is P_S, the power released by the particles to the water in which they are dispersed. A genetic algorithm minimises the sum of the squared differences between the experimental data and the calculated $T_w(t)$ curve, until the optimised P_S value is obtained. Finally, the specific loss power (for hyperthermia experiments) is calculated as:

$$SLP_h = \frac{P_S}{m_{particles}} \quad (2)$$

where $m_{particles}$ refers to the total mass of the particles (iron oxide).

Under these assumptions, P_S is considered constant. However, the thermodynamic model [31] allows to explicitly set a functional dependence of P_S on other quantities appearing in the equations, e.g. on the temperature of the water where the particles are dispersed, to account for temperature dependencies of SLP reported in literature [32]. It is therefore possible to define a new quantity, $\widetilde{P_S}$, that factorises the constant value of P_S with an explicit dependence on T_w. The resulting expression is then obtained:

$$\widetilde{P_S}(T_w) = P_S(1 - \beta(T_w - T_a)) \quad (3)$$

$\widetilde{P_S}$ is then used in the model equations [31], and its constant factor P_S is used in Eq. (2) to calculate the SLP. T_w is the temperature of the water in which the particles are dispersed and T_a is the room (ambient) temperature. T_a is measured at the beginning and at the end of a

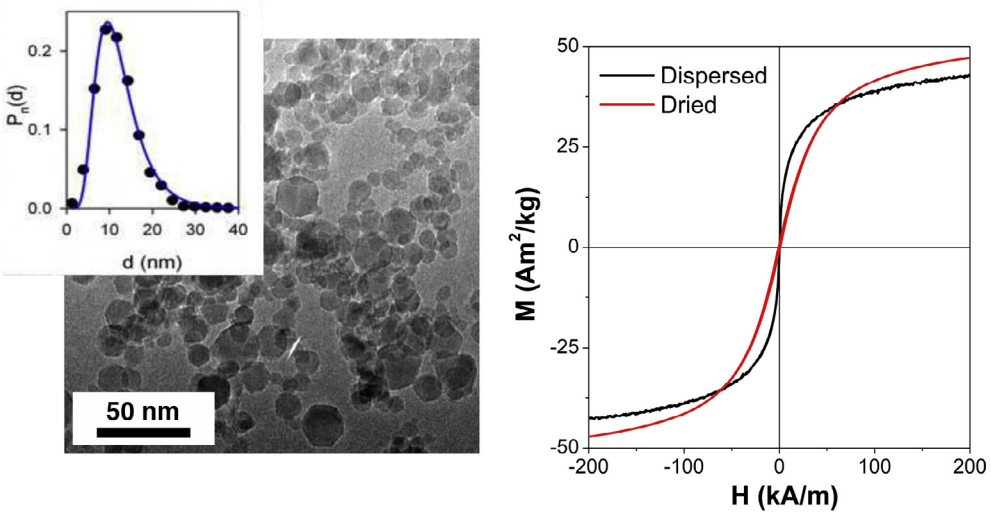

Fig. 1. Left: TEM image of the Fe-oxide particles (inset: size distribution). Right: VSM loops of dried particles (red curve) and water-dispersed particles (black curve). (For interpretation of the references to colour in this figure legend, the reader is referred to the web version of this article.)

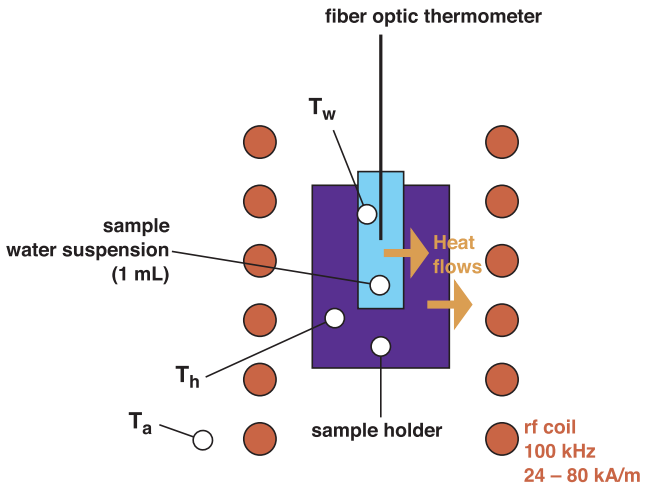

Fig. 2. Scheme of the hyperthermia setup. The orange arrows represent the heat flows, modelled by a set of differential equations described in [31]. T_w, T_h and T_a represent the temperatures of the water suspension, of the sample holder and of the external environment respectively.

hyperthermia process, and its drift as a function of time, assumed linear, is taken into account while solving the model equations reported in [31]. β is a coefficient, measured in K^{-1}, that can either be fixed to a certain value or left as a free parameter for the genetic algorithm to optimise its value together with that of P_S. In this way, when an explicit dependence of the power released by the particles to the water is taken into account, a single value of SLP can still be given, which for practical reasons refers to $T_w = T_a$.

Calorimetric measurements [33] have been conducted by means of a laboratory setup consisting in a Calvet calorimeter (see Fig. 3). Two identical cells are surrounded by solenoids applying an alternate electromagnetic field. For the experiments, the same frequency (100 kHz) as the hyperthermia setup has been used. The magnetic field intensity applicable in the calorimeter is up to ≈ 1800 A/m (the actual measured field amplitudes have been 1200 and 1750 A/m). A set of thermocouples, surrounding the cells and connected differentially, provides the signal Δ used to calculate the specific loss power (for calorimeter experiments) by means of the following expression [33]:

$$SLP_c = \frac{k\Delta}{m_{particles}} \tag{4}$$

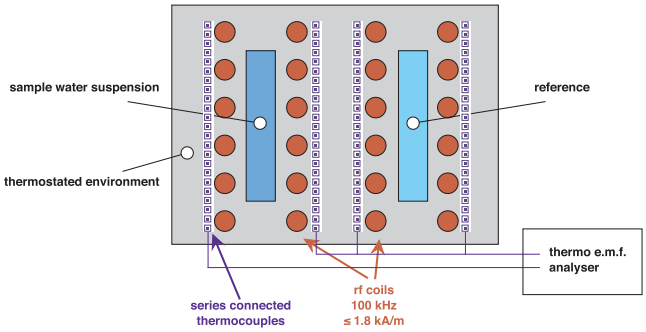

Fig. 3. Scheme of the Calvet calorimeter.

where k is the calibrated calorimeter constant.

The experiment consists in filling one cell with the water suspension of nanoparticles (total volume 0.6 mL) and acquiring Δ as a function of time both during heating (electromagnetic field switched on) and cooling (electromagnetic field switched off). Heating and cooling steps are applied until thermal equilibration of the cells is established and Δ reaches saturation. It takes approximately 15 min for either step to be accomplished. SLP is then calculated by means of Eq. (4) with Δ taken as a saturation value.

Static hysteresis loops are measured by means of a vibrating sample magnetometer (VSM) capable of generating magnetic fields up to 1.6 MA/m. The sample consists of either dry particles (dried in air at 70 °C), or a water suspension containing the particles, with a total volume of 70 μL. The hysteresis loops have been measured for different values of the maximum (vertex) magnetic field in the range 0.8–64 kA/m. At 64 kA/m a major loop is reached and static hysteresis losses no longer depend on the maximum applied field. Loops measured at a vertex field of 200 kA/m are shown in Fig. 1 demonstrating that even if losses have already saturated much earlier, the magnetisation has not yet. Loops areas have been calculated (in J/m^3) and the specific loss power (for static loops) has been obtained, by assuming a nominal density $\rho = 5000\ kg/m^3$ [34,35], according to the following expression:

$$SLP_s = \frac{A_s \nu}{\rho} \tag{5}$$

where A_s is the loop area and ν the frequency at which the loop would have been repeated if it were to be compared with a hyperthermia experiment (therefore $\nu = 100$ kHz).

Dynamic hysteresis loops have been measured by means of a

custom-built loop tracer [31] exploiting a search coil for the measurement of the applied magnetic field and two compensated pick-up coils for the measurement of the induction of the sample (70 μL of water where the particles are dispersed). The loop tracer operates at 69 kHz, and the applied fields have been equal to 14.1, 19.3, 24.6, 30.0, 34.8, 40.0 kA/m. The dynamic loops consist of 500 points equally spaced within the positive and negative vertex fields. The specific loss power (for dynamic loops) is calculated using the following expression:

$$SLP_d = \frac{A_d \nu_d}{\rho} \tag{6}$$

where A_d is the loop area (in J/m^3) and ν_d is 69 kHz. However, in order to calculate the magnetic induction of the sample, inductive loop tracers require that the sample cross section across the pick-up coils is known, in addition to the pick-up coils area. The latter quantity is known from calibration of the setup, whereas the former (the sample cross section) can be easily accessed only in bulk (solid) samples; in a water suspension the issue of finding the proper sample cross section does not have an easy solution, as the exact area fraction occupied by the nanoparticles across the pick-up coils depends on the particles size, concentration and dispersion in the solution. If the sample cross section is not accurately known, dynamic hysteresis loops can still be traced, but the vertical axis (magnetic induction) will not report accurate values. Therefore, to account for both the unknown sample cross section, and the difference between ν of hyperthermia experiments and ν_d of dynamic loops, a correction factor is applied to SLP_d to rescale its values to those of hyperthermia measurements. In particular, SLP_d measured at a magnetic field of 32 kA/m is set equal to SLP_h at the same field value, and the other values rescale consequently. This field intensity is arbitrarily chosen within the extrema of the measurement ranges of hyperthermia and dynamic loops setups. It is very important to remark that this procedure of rescaling the dynamic losses to the hyperthermia ones could be acceptable if the two experimental setups, dynamic loops tracer and hyperthermia system, were operating at the same frequency. As they are not, in principle frequency-dependent effects superimpose to the field-dependent ones, but with our procedure we assume that SLP_d is proportional to SLP_h at any applied field. While this assumption is not generally true, in our case it is supported by the fact that the complex magnetic permeability of iron oxides is usually frequency-independent up to several hundreds kHz [36,37].

3. Results and discussion

The results of a typical hyperthermia experiment, performed at a magnetic field intensity of 40 kA/m, are reported in Fig. 4. The experimental data (green symbols) show the temperature increase of the water suspension, having a concentration of 4.65 mg/mL (total solid mass of Fe_2O_3), that is heated by the alternating electromagnetic field. After 3600 s of treatment, the field is switched off and the temperature recovers to room temperature after a certain time. In order to calculate the specific loss power, the genetic algorithm has been run to optimise the power P_S lost by the particles, with a coefficient $\beta = 0$ (see Eq. (3)). The best solution (see orange curve of Fig. 4), however, is not able to adequately reproduce the experimental points, that contrary to other particles suspensions studied in literature with the same setup and method (see e.g. [30,31]) has a significantly faster increase of temperature at the beginning of the treatment, followed by a faster "saturation" to the limit equilibrium temperature. Instead, by letting the genetic algorithm optimise also the value of β, a satisfactory representation of the experimental data has been obtained (blue line), resulting in a SLP value, calculated according to Eq. (2), equal to 214.4 W/g. Similar results, with β values ranging in the interval $0.0139 - 0.0166$, have been obtained for all studied field intensities.

The heat flux results obtained with the Calvet calorimeter are reported in Fig. 5. The experimental data show the calorimetric signal in the battery of thermocouples (Δ) under the application of an

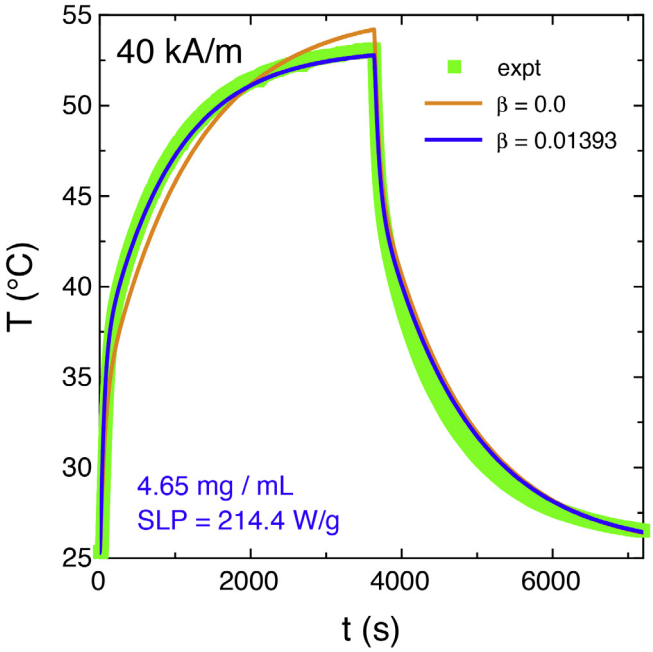

Fig. 4. Hyperthermia measurements performed at a magnetic field intensity of 40 kA/m on a water suspension with a concentration of 4.65 mg/mL. Green squares: experimental data. Blue and orange lines: optimised numerical results obtained with β equal to 0.01393 and 0.0 respectively (see Eq. (3)). (For interpretation of the references to colour in this figure legend, the reader is referred to the web version of this article.)

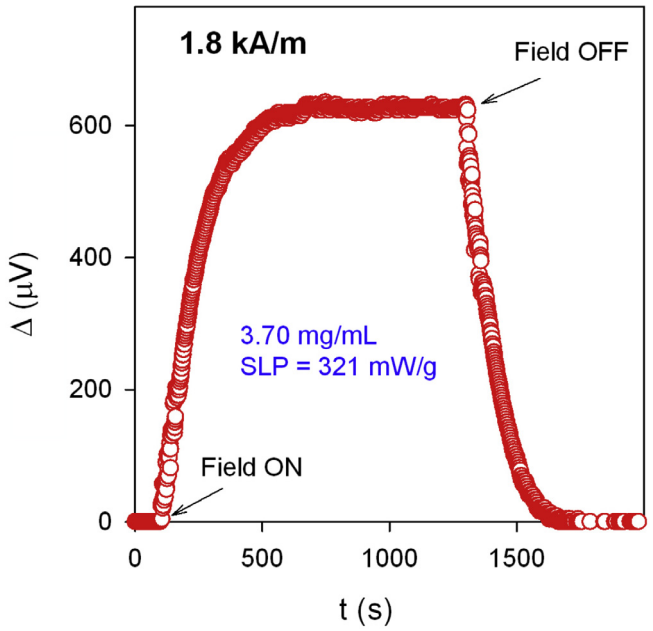

Fig. 5. Calorimetric measurements performed at a magnetic field intensity of 1.8 kA/m on a water dispersion of particles with a concentration of 3.70 mg/mL. Δ is the calorimeter signal used to calculate SLP_c according to Eq. (4).

electromagnetic field of 1.8 kA/m irradiating a water dispersion of particles with a concentration of 3.70 mg/mL of γ-Fe_2O_3 particles. This slight reduction of concentration with respect to the hyperthermia measurements should not be significant in terms of variations of interparticle interactions, which could affect the SLP, as the rather diluted dispersion, and the good stability of the colloidal suspension ensure a negligible presence of agglomerates in both experiments. Indeed, dipole-dipole interactions can significantly affect dynamic losses in water-

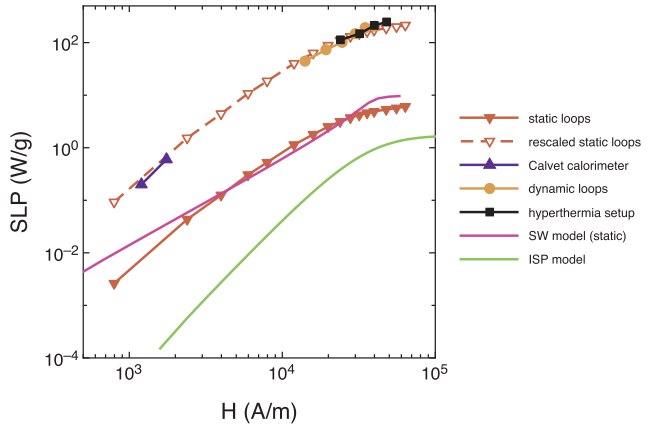

Fig. 6. Specific loss power values obtained with the different techniques. Black squares: hyperthermia setup. Red triangles pointing down: static hysteresis loops. Open red triangles pointing down with dashed line: same curve, rescaled to coincide with the black symbol at 32 kA/m. Blue triangles pointing up: Calvet calorimeter. Orange circles: dynamic loops. Green curve: SLP calculated according to the interacting superparamagnetic model (ISP) [42] with an interaction field of 11.9 kA/m. Magenta curve: SLP calculated according to the Stoner-Wohlfarth (SW) model corrected for magnetic interactions, using $\langle K \rangle = 1.4{\cdot}10^4$ J/m^3, $r = 0.0045$ and $N = 0.25$ in Eq. (7).

dispersed particles systems, as interacting particles have a reduced ability to rotate under the influence of the magnetic field and their magnetic susceptibility is also significantly affected. However, it is only under major variations of concentration, and for much higher concentration values, that these effects can no longer be neglected [38]. As the electromagnetic field was turned on, the irradiation of heat by oscillating dipoles resulted in the signal Δ of the thermocouples, which reached saturation when all of the power released by heating was dissipated from the measurement cell along the thermocouples, reaching an equilibrium state. The signal at the saturation level corresponds to the equilibrium heat flux from the suspension in the 100 kHz electromagnetic field. As the field was turned off, the heat flux from the cell with suspension vanished to the baseline of the calorimeter. The resulting SLP values are calculated according to Eq. (4).

The SLP values obtained at different applied magnetic field intensities using the available techniques (hyperthermia, Calvet calorimeter, static loops, dynamic loops) are summarised in Fig. 6. Hyperthermia and Calvet calorimeter data are represented by black and blue symbols respectively. The dynamic loops data have been rescaled to let the point at a vertex field of 32 kA/m coincide with the point of the hyperthermia experiments at the same field, as discussed in Section 2. The red triangles, connected by a continuous line, are the SLP values calculated from static hysteresis loops. This curve lies evidently below the other data, as dynamic effects do not take place in these conditions. Nonetheless, static loops allow easily to explore a wide range of vertex field values, overlapping both the field regions of the Calvet calorimeter and of the hyperthermia setup.

For the dynamic hysteresis loops, the origin of the observed hysteresis emerges. In systems made of nanoparticles dispersed in fluids, Brown and Néel relaxation effects can be responsible for dynamic hysteresis when excitation periods are comparable to the respective relaxation times, which are respectively equal to $\tau_B = \frac{3\eta V_h}{k_B T}$ and $\tau_N = \tau_0 e^{\frac{KV}{k_B T}}$, where η is the water viscosity ($\approx 1.01{\cdot}10^{-3}$ kg m^{-1} s^{-1}), V_h is the hydrodynamic volume, k_B is the Boltzmann constant, T is the temperature, $\tau_0 \approx 3{\cdot}10^{-9}$ s, K is the magnetic anisotropy and V is the particles volume [39,40]. If we assume that $V_h = V$, a temperature $T = 300$ K, an average radius of 6 nm and an anisotropy constant of $5{\cdot}10^3$ J/m^3 [41], the relaxation times turn out to be $\tau_B \approx 6.6{\cdot}10^{-7}$ s and $\tau_N \approx 3.0{\cdot}10^{-9}$ s, with an effective $\tau = \frac{\tau_B \tau_N}{\tau_B + \tau_N} = 1{\cdot}10^{-9}$ s. At the frequency at which the dynamic loops are measured, the relaxation time turns out to be much shorter than the period of measurement, therefore making both Brown and Néel effects negligible in determining the power losses. Instead, the observed loop area must come from hysteresis losses. As discussed earlier, it is difficult to accurately assess the magnetic induction of the water suspension of magnetic nanoparticles, therefore we refer the dynamic measurements to the hyperthermia ones. Following the same discussion reported in Section 2, we assume that dynamic effects rescale the static hysteresis loops areas by a constant amount, e.g. a proportionality factor, and therefore we multiply the static loops areas by a certain quantity to obtain the area that dynamic loops, performed at 100 kHz, would have. This assumption, that in general cannot be valid for a single proportionality factor independent on the sample and the measurement conditions, in our particular case is supported by the usually observed independence on frequency of the complex magnetic permeability in iron oxides up to several hundreds kHz [36,37]. The proportionality factor, to be determined experimentally, would then include the contributions of any dynamic effects, and would not depend on the magnetic field intensity. If this assumption is considered to hold true, the curve of the SLP values calculated from static loops can be rescaled, for example by imposing that it coincides with the hyperthermia data at a certain field value. The result, by arbitrarily imposing a perfect overlap for the field equal to 32 kA/m in analogy to what we have done for the dynamic loops data, is shown in Fig. 6 in the open red symbols connected with a dashed line. Even if the overlap with just one experimental point is forced, all available points measured with hyperthermia setup, Calvet calorimeter and dynamic loops perfectly agree with the rescaled SLP from static loops. Under the assumption stated above, the SLP value calculated from static loops, provided that it can be rescaled to at least one point taken at the proper frequency, can be used both to assess the consistency of the data taken on the same sample from different setups and experiments, and to extrapolate SLP values to field intensities that cannot be covered with the available experimental setup, for example to help comparing data obtained on different samples with different equipments.

The static loops energy losses can also be investigated by means of suitable hysteresis models dealing with magnetic nanoparticles. Multiple approaches can be exploited, depending on the dominant mechanism driving the magnetisation processes in the nanoparticles. If they are superparamagnetic, multi-body dipolar interactions are known to induce a hysteresis [42] which contributes to their energy losses. These are accounted for the so-called “interacting superparamagnetic model” (ISP) [42], that demonstrates how dipolar interactions among magnetic nanoparticles can induce an hysteresis on an otherwise superparamagnetic system. The model has been successfully used on a variety of nanoparticles systems [43,44] where deviations from the expected superparamagnetic behaviour were experimentally observed. In Fig. 6, the green curve corresponds to the static loop area calculated using the ISP model. The magnetic moment of each particle has been taken equal to 20000 μ_B, consistent with the average particle size obtained from TEM images. The mean interaction field, in Fig. 6, has been set to 11.9 kA/m, which is even larger the values often found in literature when systems of magnetic nanoparticles obeying the ISP model are discussed [42]. The green curve is evidently very far from overlapping the red triangles, representing the static loops areas measured by VSM. Even by increasing the mean interaction field well above any physically meaningful value, the green curve cannot be forced to overlap the static loops experimental data; this fact proves that the ISP model is unable to explain the energy losses of our ensemble of particles.

For this reason, and also to account for the fact that most of the particles, in agreement with structural data, are probably large enough to be below their blocking temperature even at room temperature, an alternative choice can be searched in the field of vector models. Among the numerous approaches proposed to deal with this kind of phenomenology [45], we have followed the line indicated by the Stoner-

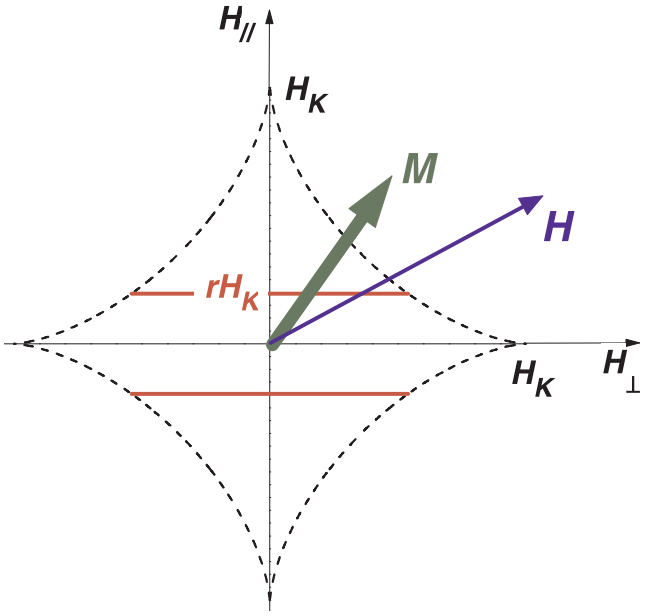

Fig. 7. The astroid representation. In the native formulation of the Stoner-Wohlfarth model, the stability regions are separated by a boundary of equation $H_{//}^{2/3} + H_{\perp}^{2/3} = H_K$ (dashed lines), being H_K the anisotropy field. The red thresholds delimit a "truncated astroid" that defines a different $(H_{\perp}, H_{//})$ plane partition, where the new stability regions suitably account for the γ-Fe_2O_3 nanoparticle switches.

Wohlfarth (SW) approach, and accordingly considered the system as an ensemble of uniaxial anisotropy particles, with anisotropy constant K, and direction uniformly distributed in space [46]. Each particle is described by a vector operator (endowed with hysteresis, and for this reason often called "hysteron"), which gives the orientation of the local magnetization M, in equilibrium under the antagonist effect of the torques associated to the anisotropy and the Zeeman energies. The behavior of each operator is efficiently described by means of the so-called astroid representation (Fig. 7). Accordingly, we consider a plane identified by the axes $H_{\perp}$ and $H_{//}$ (the anisotropy direction), defined by the projections of the local field H, where the astroid boundary of equation $H_{//}^{2/3} + H_{\perp}^{2/3} = H_K$ (dashed curves in Fig. 7) splits the $(H_{\perp}, H_{//})$ plane in two simply connected regions. When H points inside the astroid (of vertexes given by the anisotropy field $H_K = 2K/J_s$, being J_s the saturation polarisation) two equilibrium orientations for M are allowed, whereas only one is available if H points outside. By means of this tool one is able to follow the orientation of M in response to the evolution of H with time.

However, the SW model, in its native formulation, only contemplates coherent reversible M rotations, when the H *vs.* time path remains confined inside or outside the astroid, or irreversible rotations, when H exits it. Nevertheless, a more complicated mechanism leading to the magnetisation reversal operates here, and some refinement is then needed, similarly to the cases discussed in [47,48]. To this end, we postulate that in each hysteron the transition between the two stable magnetisation positions can occur at a boundary different from the astroid. This is done by considering a so-called "truncated astroid", where a new stability region is introduced, delimited by a threshold appearing at rH_K (red thick segments in Fig. 7), with r a parameter lower than 1 [46].

In order to properly reproduce the experimental static loops, we have also assumed the presence of a magnetostatic interaction among the particles, leading to decrease of the magnetisation [49]. This effect is described by means of a mean-field approach, and hence the particles experience an effective field $H = H_a + N\langle M\rangle$, where $\langle M\rangle$ is the average magnetisation of the system, and N a suitable parameter. The area of the (H, M) hysteresis loop given by each hysteron operator represents the energy loss per cycle of the corresponding particle, and the energy loss of the whole system is known after integration over each contribution, with the following probability density function for the anisotropy:

$$f_K(K) = \left(\frac{2}{\langle K\rangle}\right)^2 K e^{-\frac{2}{\langle K\rangle}K} \tag{7}$$

which has been found to suitably describe the anisotropy values distribution [45,50]. In Eq. (7) $\langle K\rangle$ is the average value of the particle anisotropy. In Fig. 6 the magenta curve represents the calculated losses for the modified SW model with the following parameters: $\langle K\rangle = 1.4{\cdot}10^4$ J/m^3, $r = 0.0045$, $N = 0.25$. While the experimental data could not be perfectly reproduced, especially at small vertex (peak) field amplitudes, the overall behaviour of the energy losses as a function of the maximum applied field is reasonably obtained.

It is worth remarking that any attempt to reproduce the experimental static energy losses with very simple models, such as the modified SW one, must face with the complexity of the nanoparticles system. Not only the nanoparticles may have slightly varying stoichiometry (oxidation state) and size, and magnetically interact, but their magnetisation most probably cannot be considered homogeneous either [51–56]. In order to more accurately model their magnetic behaviour, in fact, a core@shell system [57–61,12] should probably be considered, taking into account the presence of a shell a few atoms thick whose spins are misaligned with those of the core, forming a disordered, possibly frustrated spin-glass state. Its presence affects the saturation magnetisation of the particles, but also their magnetic anisotropy and the way the magnetisation reverses as a function of the applied magnetic field. The modified SW model must therefore be considered as a simple tool to reasonably reproduce the static losses as a function of the vertex field, for physically meaningful values of its parameters, whereas more accurate results can probably be obtained with much more complex models.

4. Conclusions

Specific loss power has been measured on γ-Fe_2O_3 nanoparticles by using different techniques spanning a wide range of applied magnetic field intensities. Comparison of the data obtained by the different methods has been made possible through static hysteresis loops, that in spite of neglecting all dynamic effects, can easily cover the whole range of magnetic field intensities exploited by the dynamic techniques. The Calvet calorimeter, the hyperthermia setup and the dynamic loops turned out to provide consistent results in spite of SLP values spanning almost 3 orders of magnitude because of the difference in applied field intensities. The temperature dependence of the SLP has been explicitly taken into account in hyperthermia measurements. The investigation of the static energy losses of the ensemble of particles by exploiting simple mean-field theoretical models revealed that a modified Stoner-Wohlfarth approach, with a suitable interaction field, could satisfactorily reproduce the vertex (peak) field dependence of the energy losses, revealing a complex many-body behaviour of the nanoparticles. Static models and measurements, in spite of neglecting all dynamic components of energy losses, have been nonetheless revealed to be useful tools for covering large intervals of vertex field values, not easily accessible with single dynamic techniques (hyperthermia, calorimeters), providing a tool for connecting results obtained with different setups in different regimes.

Our analysis is limited to just one frequency value for hyperthermia and dynamic loops measurements. However, in the frequency interval usually investigated for magnetic hyperthermia applications (10 kHz–1 MHz), the effects responsible for the power losses of a magnetic nanoparticles suspension do not change; therefore, we expect that our analysis would remain consistent if the frequency values were

changed within this interval, with the only important notice that the rescaling of the dynamic loops to the static ones must be re-determined (as dynamic losses are frequency dependent) for every explored frequency value, unless a model describing the evolution of hysteresis losses with field frequency is available.

Acknowledgments

This work was supported in part by Russian Science Foundation grant 18-19-00090. This work was funded in part by the EMPIR program co-financed by the Participating States and from the European Union's Horizon 2020 research and innovation program, project 16NRM044 "MagNaStand".

References

[1] Q.A. Pankhurst, J. Connolly, S.K. Jones, J. Dobson, J. Phys. D: Appl. Phys. 36 (2003) R167–R181.
[2] Y.-W. Jun, J.-W. Seol, J. Cheon, Acc. Chem. Res. 41 (2) (2008) 179–189.
[3] P. Moroz, S.K. Jones, B.N. Gray, J. Surg. Oncol. 77 (2001) 259–269.
[4] G.V. Kurlyandskaya, E. Fernández, A.P. Safronov, F.A. Blyakhman, A.V. Svalov, A. Burgoa Beitia, I.V. Beketov, J. Magn. Magn. Mater. 441 (2017) 650–655.
[5] S. Kennedy, C. Roco, A. Délérisa, P. Spoerria, C. Cezara, J. Weavera, H. Vandenburghd, D. Mooney, Biomaterials 161 (2018) 179–189.
[6] R. Glaser, Biophysics, Springer Verlag, Heidelberg, Germany, 1999, p. 362.
[7] J.H. Grossman, S.E. McNeil, Nanotechnology in cancer medicine, Phys. Today 65 (2012) 38–42.
[8] Y.-W. Jun, J.-W. Seo, J. Cheon, Acc. Chem. Res. 41 (2008) 179.
[9] I.V. Beketov, A.P. Safronov, A.I. Medvedev, J. Alonso, G.V. Kurlyandskaya, S.M. Bhagat, AIP Adv. 2 (2012) 022154.
[10] V.V. Osipov, V.V. Platonov, M.A. Uimin, A.V. Podkin, Tech. Phys. 57 (2012) 543.
[11] G.V. Kurlyandskaya, S.M. Bhagat, A.P. Safronov, I.V. Beketov, A. Larranaga, AIP Adv. 1 (2011) 042122.
[12] A.P. Safronov, I.V. Beketov, S.V. Komogortsev, G.V. Kurlyandskaya, A.I. Medvedev, D.V. Leiman, A. Larranaga, S.M. Bhagat, AIP Adv. 3 (2013) 052135.
[13] I.D. Morrison, S. Ross, Colloidal Dispersions: Suspensions, Emulsions and Foams, Wiley, NewYork, 2002.
[14] J.P. Novoselova, A.P. Safronov, O.M. Samatov, I.V. Beketov, H. Khurshid, Z. Nemati, H. Srikanth, T.P. Denisova, R. Andrade, G.V. Kurlyandskaya, IEEE Trans. Magn. 50 (2014) 4600504.
[15] F. Spizzo, P. Sgarbossa, E. Sieni, A. Semenzato, F. Dughiero, M. Forzan, R. Bertani, L. Del Bianco, Nanomaterials 7 (2017) 373.
[16] C.H. Kuo, Y.C. Liu, C.M.J. Chang, J.H. Chen, C. Chang, C.J. Shieh, Carbohydr. Polym. 87 (2012) 2538.
[17] I.S. Tyukova, A.P. Safronov, A.P. Kotelnikova, D.Yu. Agalakova, Polym. Sci. Ser. A 56 (2014) 498.
[18] G.V. Kurlyandskaya, L.S. Litvinova, A.P. Safronov, V.V. Schupletsova, I.S. Tyukova, O.G. Khaziakhmatova, G.B. Slepchenko, K.A. Yurova, E.G. Cherempey, N.A. Kulesh, R. Andrade, I.V. Beketov, I.A. Khlusov, Sensors 17 (2017) 2605.
[19] P. Lemal, C. Geers, B. Rothen-Rutishauser, M. Lattuada, A. Petri-Fink, Mater. Today: Proc. 4 (2017) S107.
[20] R.R. Wildeboer, P. Southern, Q.A. Pankhurst, J. Phys. D: Appl. Phys. 47 (2014) 495003.
[21] S. Dutz, R. Hergt, Nanotechnology 25 (2014) 452001.
[22] I.M. Obaidat, B. Issa, Y. Haik, Nanomaterials 5 (2015) 63.
[23] A. Périgo, G. Hemery, O. Sandre, D. Ortega, E. Garaio, F. Palazola, F.J. Teran, Appl. Phys. Rev. 2, 041302.
[24] M. Latorre, C. Rinaldi, PRHJS 28 (2009) 227.
[25] G. Vallejo-Fernandez, O. Whear, A.G. Roca, S. Hussain, J. Timmis, V. Patel, K. O'Grady, J. Phys. D: Appl. Phys. 46 (2013) 312001.
[26] E.L. Verde, G.T. Landi, M.S. Carriao, A.L. Drummond, J.A. Gomes, E.D. Vieira, M.H. Sousa, A.F. Bakuzis, AIP Adv. 2 (2012).
[27] Yu.A. Kotov, J. Nanoparticle Res. 5 (2003) 539.
[28] E.L. Crow, K. K. Shimizu, Lognormal Distributions, Theory and Applications, Statistics: Textbooks and Monographs 88, Marcel Dekker, New York, 1998, p. xvi +387.
[29] T.B.L. Kirkwood, Geometric means and measures of dispersion, Biometrics 35 (1979) 908–909.
[30] M. Coïsson, G. Barrera, F. Celegato, L. Martino, F. Vinai, P. Martino, G. Ferraro, P. Tiberto, J. Magn. Magn. Mater. 415 (2016) 2.
[31] M. Coïsson, G. Barrera, F. Celegato, L. Martino, S.N. Kane, S. Raghuvanshi, F. Vinai, P. Tiberto, Biochim. Biophys. Acta 1861 (2017) 1545.
[32] S. Merabia, S. Shenogin, L. Joly, P. Keblinski, J.-L. Barrat, PNAS 106 (2009) 15113.
[33] Iu.P. Novoselova, A.P. Safronov, O.M. Samatov, G.V. Kurlyandskaya, AIP Conf. Proc. 1767 (2016) 020016.
[34] K. Landfester, L.P. Ramŕez, J. Phys.: Condens. Matter 15 (2003) S1345.
[35] J. Vidal-Vidal, J. Rivas, M.A. López-Quintela, Colloids Surf. A: Physicochem. Eng. Aspects 288 (2006) 44.
[36] F. Fiorillo, C. Beatrice, M. Coïsson, L. Zhemchuzhna, IEEE Trans. Magn. 45 (2009) 4242.
[37] H. Yun, X. Liu, T. Paik, D. Palanisamy, J. Kim, W.D. Vogel, A.J. Viescas, J. Chen, G.C. Papaefthymiou, J.M. Kikkawa, M.G. Allen, C.B. Murray, ACS Nano 8 (2014) 12323.
[38] S. Ota, T. Yamada, Y. Takemura, J. Appl. Phys. 117 (2015) 17D713.
[39] R. Hergt, R. Hiergest, I. Hilger, W.A. Kaiser, Y. Lapatnikov, S. Margel, U. Richter, J. Magn. Magn. Mater. 270 (2004) 345.
[40] A.E. Deatsch, B.J. Evans, J. Magn. Magn. Mater. 354 (2014) 163.
[41] A.I. Figueroa, J. Bartolomé, L.M. García, F. Bartolomé, A. Arauzo, A. Millán, F. Palaciom, Phys. Proc. 75 (2015) 1050.
[42] P. Allia, M. Coïsson, M. Knobel, P. Tiberto, F. Vinai, Phys. Rev. B 60 (1999) 12207.
[43] J.B. Souza Jr., L.C. Varanda, Nanotechnology 29 (2018) 065604.
[44] P. Allia, G. Barrera, P. Tiberto, T. Nardi, Y. Leterrier, M. Sangermano, J. Appl. Phys. 116 (2014) 113903.
[45] C. Appino, C. Ragusa, F. Fiorillo, Int. J. Appl. Electromagn. Mech. 44 (2014) 355.
[46] C. Appino, M. Valsania, V. Basso, Physica B (Cond. Matt.) 275 (2000) 103.
[47] H.A.J. Cramer, J. Magn. Magn. Mater. 88 (1990) 194.
[48] F. Ossart, R. Davidson, S.H. Charap, IEEE Trans. Magn. 30 (1994) 4260.
[49] A. Stancu, C. Papusoi, IEEE Trans. Magn. 30 (1994) 4308.
[50] C. Appino, F. Fiorillo, J. Appl. Phys. 76 (1994) 5371.
[51] D. Caruntu, G. Caruntu, C.J. O'Connor, J. Phys. D: Appl. Phys. 40 (2007) 5801.
[52] D.A. Garanin, H. Kachkachi, Phys. Rev. Lett. 90 (2003) 065504.
[53] D.S. Schmool, R. Rocha, J.B. Sousa, J.A.M. Santos, G. Kakazei, J. Magn. Magn. Mater. 300 (2006) e331.
[54] M.P. Morales, S. Veintemillas-Verdaguer, M.I. Montero, C.J. Serna, A. Roig, Ll. Casas, B. Martínez, F. Sandiumenge, Chem. Mater. 11 (1999) 3058.
[55] D. Peddis, C. Cannas, G. Piccaluga, E. Agostinelli, D. Fiorani, Nanotechnology 21 (2010) 125705.
[56] E. Tronc, A. Ezzir, R. Cherkaoui, C. Chanác, M. Noguès, H. Kachkachi, D. Fiorani, A.M. Testa, J.M. Grenèche, J.P. Jolivet, J. Magn. Magn. Mater. 221 (2000) 63.
[57] R.H. Kodama, A.E. Berkowitz, E.J. McNiff, S. Foner, Phys. Rev. Lett. 77 (1996) 394.
[58] J.M.D. Coey, Magnetism and Magnetic Materials, Cambridge University Press, New York, 2010, p. 628.
[59] H.M. Lu, W.T. Zheng, Q. Jiang, J. Phys. D: Appl. Phys. 40 (2007) 320.
[60] T.N. Shendruk, R.D. Desautels, B.W. Southern, J. van Lierop, Nanotechnology 18 (2007) 455704.
[61] Y. Komorida, M. Mito, H. Deguchi, S. Takagi, A. Millán, N.J.O. Silva, F. Palacio, Appl. Phys. Lett. 94 (2009) 202503.